Influence of confinement on the orientational phase transitions in the lamellar phase of a block-copolymer melt under shear flow

A. N. Morozov,[1,2,*] A. V. Zvelindovsky,[2] and J. G. E. M. Fraaije[2]
[1]*Faculty of Mathematics and Natural Sciences, University of Groningen, Nijenborgh 4, 9747 AG Groningen, The Netherlands*
[2]*Soft Condensed Matter Group, LIC, Leiden University, P.O. Box 9502, 2300 RA Leiden, The Netherlands*
(Received 18 April 2001; published 18 October 2001)

In this paper, we incorporate some real-system effects into the theory of orientational phase transitions under shear flow [M. E. Cates and S. T. Milner, Phys. Rev. Lett. **62** 1856 (1989) and G. H. Fredrickson, J. Rheol. **38**, 1045 (1994)]. In particular, we study the influence of the shear-cell boundaries on the orientation of the lamellar phase. We predict that at low shear rates, the parallel orientation appears to be stable. We show that there is a critical value of the shear rate at which the parallel orientation loses its stability and the perpendicular one appears immediately below the spinodal. We associate this transition with a crossover from the fluctuation to the mean-field behavior. At lower temperatures, the stability of the parallel orientation is restored. We find that the region of stability of the perpendicular orientation rapidly decreases as shear rate increases. This behavior might be misinterpreted as an additional perpendicular to parallel transition recently discussed in literature.

DOI: 10.1103/PhysRevE.64.051803 PACS number(s): 83.80.Uv, 64.60.Ht, 83.50.Ax, 47.20.Hw

I. INTRODUCTION

When subjected to a shear flow, *AB* block-copolymer melts exhibit an orientational phase behavior that is absent in equilibrium. A system under shear shows not only transitions between different morphologies (typically lamellar, hexagonal, cubic, and gyroid [1,2]), but also transitions between different *orientations* of these morphologies with respect to the shear geometry. Experimental literature extensively discusses this effect for lamellar [3,4] and hexagonal phases [5,6].

The theoretical description of the lamellar reorientation was developed in [7,8]. The same method was applied in [9] to study the hexagonal pattern. In these theories, orientational transitions appear as a result of the interaction of shear flow with critical fluctuations in melt. There are two distinct regimes: a slow flow only slightly perturbs the fluctuation spectrum while a fast flow significantly dumps fluctuations, restoring the mean-field behavior in the limit of infinite shear rate $D\rightarrow\infty$. Correspondingly, the parallel lamellae (their normal is parallel to the shear gradient direction) are found to be stable in the small shear rate regime, while the perpendicular lamellae (their normal is perpendicular to both the gradient and flow directions) are stable at high shear rates. Fredrickson has shown that if one takes into account the difference in viscosities of the pure melt components, the perpendicular phase loses its stability at low enough temperatures and the parallel orientation is restored. Schematically, this behavior is summarized in Fig. 1.

However, there is an experimental evidence that this picture is not complete. At very high shear rates, the parallel orientation was found to be the only stable one [10,11]. This cannot be explained in the discussed framework of [8], since it predicts the stability region for the perpendicular phase *to increase* as $D\rightarrow\infty$.

In this paper, we propose an explanation of the additional transition (*C* transition in Fig. 1). We argue that the missing element of the theory is the interaction of the block copolymer melt with the walls of the shear cell. We consider a block copolymer film confined in between two walls in the gradient direction and subjected to a steady shear flow. Usually the distance between the interfaces in the other two directions is much larger and we ignore their influence. This model will predict the parallel orientation to be stable in the $D\rightarrow\infty$ limit since the influence of shear and fluctuations vanishes in this limit. The only symmetry-breaking factor is then the wall-copolymer interaction that stabilizes the parallel orientation [12,13]. The complex behavior at lower shear rateswill arise from the interplay of three factors: shear flow,

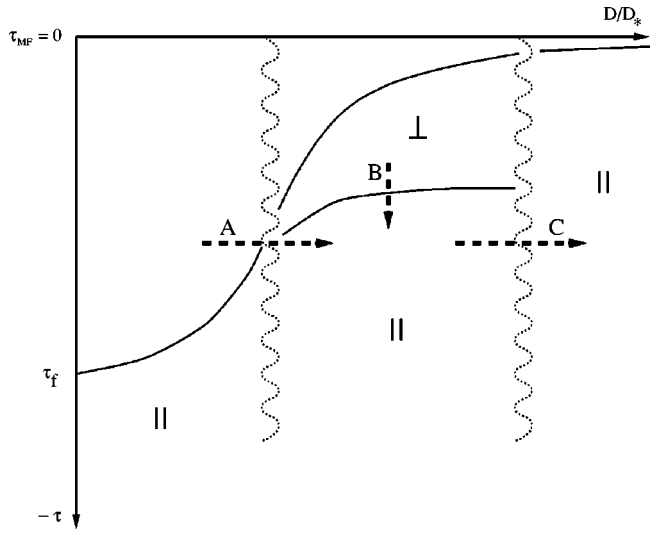

FIG. 1. Schematic phase diagram ''temperature vs shear rate'' as a compilation of the theoretical predictions by Fredrickson and the experimentally observed *C* transition. The order-disorder transition line behaves as $\tau\sim D^2$ for small shear rates *D* and $\tau\sim D^{-1/3}$ for $D\rightarrow\infty$. The *B*-transition line levels off in Fredrickson's theory.

*Email address: a.n.morozov@chem.rug.nl

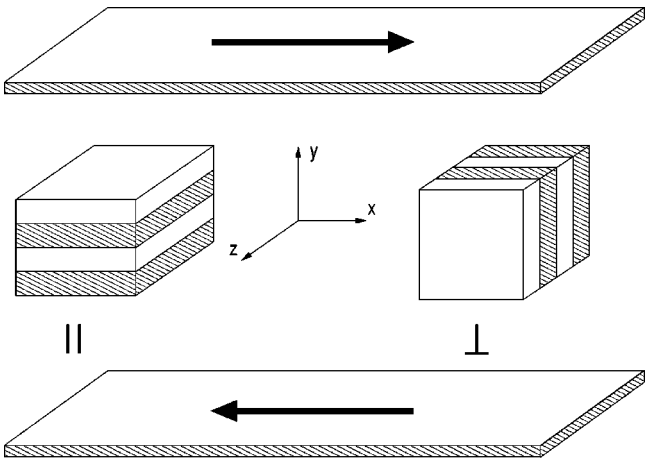

FIG. 2. Orientations of the lamellar phase in a simple shear flow. The axes of the coordinate system correspond to the shear geometry: x is the flow direction ($\mathbf{v}$), y is the gradient direction (∇v_x), and z is the vorticity direction ($\nabla \times \mathbf{v}$). In the parallel orientation, the normal to the lamellar layers is oriented parallel to the gradient direction, in the perpendicular—to the vorticity direction. The walls in y direction interact with the melt and prefer one of the components.

fluctuations, and wall-melt interactions.

We admit that the influence of the surface interactions is possibly small. However, Balsara *et al.* reported [14] that in the absence of shear, the walls of their shear cell induced the parallel alignment through the whole 0.5 mm sample, although the lamellar spacing is somewhat four orders of magnitude smaller. Under shear, Laurer *et al.* [15] observed that independent of the bulk orientation, there is always a near-surface layer of the parallel lamellae that penetrates up to 2 μm into the bulk. Thus, even a weak symmetry-breaking field can be crucial in the absence of other factors.

We also want to mention that the equilibrium theory of block-copolymer melt ordering near surfaces is well developed [12,13,16–22]. Some questions about dynamics of such an ordering were addressed in [23,20]. However, until now this theory was never applied to nonequilibrium systems.

Our paper is organized as follows. In Sec. II, we derive the equations governing the dynamics of the melt and construct a nonequilibrium potential whose minimal value will determine the stable orientation. In the first part of Sec. III, we estimate the shear rate of the A transition while the other two transitions (B and C) are analyzed in the second part. In conclusion we discuss in detail properties of the obtained phase diagram. In the Appendix we provide an example clarifying the role of thermal fluctuations.

II. DYNAMIC EQUATIONS

Let us consider a block-copolymer melt confined in between two surfaces in the y direction. It is also subjected to a steady-shear flow $\mathbf{v}=Dy\,\mathbf{e}_x$ (see Fig. 2). We ignore any alteration of this velocity profile and assume that it is kept through the whole system. We choose the local deviation of composition from its average to be an order-parameter $\phi(\mathbf{r})$ and define its Fourier transform as

$$\phi(\mathbf{k})=\int d\mathbf{r}\, e^{-i\mathbf{k}\cdot\mathbf{r}}\phi(\mathbf{r}) \quad \text{and} \quad \phi(\mathbf{r})=\int_k e^{i\mathbf{k}\cdot\mathbf{r}}\phi(\mathbf{k}), \tag{2.1}$$

where

$$\int_k \equiv \frac{1}{L}\sum_{k_y}\int\frac{dk_x dk_z}{(2\pi)^2} \quad \text{and} \quad \int d\mathbf{r} \equiv \int_{-\infty}^{\infty}dx\int_{-L/2}^{L/2}dy\int_{-\infty}^{\infty}dz. \tag{2.2}$$

It is convenient to work in dimensionless units and we rescale lengths and wave vectors: $\mathbf{r}\to b^{-1}\mathbf{r}$ and $\mathbf{k}\to b\,\mathbf{k}$, b being the size of a monomer.

Following [24,7,8] we assume that the dynamics under shear flow is governed by the Fokker-Planck equation:

$$\frac{\partial P[\phi,t]}{\partial t}=\int d\mathbf{r}\frac{\delta}{\delta\phi(\mathbf{r})}\left[\mu\left(\frac{\delta}{\delta\phi(\mathbf{r})}+\frac{\delta\mathcal{H}}{\delta\phi(\mathbf{r})}\right)+Dy\frac{\partial\phi}{\partial x}\right]P[\mathbf{r},t], \tag{2.3}$$

where $P[\phi,t]$ is the probability to realize the order-parameter profile $\phi(\mathbf{r})$ at time t, and μ is an Onsager coefficient. In the Appendix, we provide arguments for using the Fokker-Planck equation instead of any other deterministic equation.

In Eq. (2.3), the Hamiltonian $\mathcal{H}$ consist of two contributions: the bulk Hamiltonian derived by Leibler [2]

$$\begin{aligned}N\mathcal{H}_L[\phi]=&\tfrac{1}{2}\int_q\Gamma_2(q)\phi(\mathbf{q})\phi(-\mathbf{q})\\&+\frac{1}{3!}\int_{q_1}\int_{q_2}\int_{q_3}\Gamma_3(\mathbf{q}_1,\mathbf{q}_2,\mathbf{q}_3)\phi(\mathbf{q}_1)\phi(\mathbf{q}_2)\phi(\mathbf{q}_3)\\&+\frac{1}{4!}\int_{q_1}\int_{q_2}\int_{q_3}\int_{q_4}\Gamma_4(\mathbf{q}_1,\mathbf{q}_2,\mathbf{q}_3,\mathbf{q}_4)\\&\times\phi(\mathbf{q}_1)\phi(\mathbf{q}_2)\phi(\mathbf{q}_3)\phi(\mathbf{q}_4),\end{aligned} \tag{2.4}$$

and the surface energy [12,13]

$$N\mathcal{H}_s=\int d\mathbf{r}\left[-H_1\phi(\mathbf{r})+\frac{a_1}{2}\phi(\mathbf{r})^2\right]\times\left[\delta\left(y+\frac{L}{2}\right)+\delta\left(y-\frac{L}{2}\right)\right], \tag{2.5}$$

where N is a number of monomers in a molecule, $H_1\sim(\chi N)_{cop\text{-}surf}$ is the strength of the interaction between the surface, and the copolymer melt and a_1 describes the additional interaction in the melt induced by the presence of the surface (it changes the local temperature in the vicinity of the surface). Our goal is to construct a real-space version of the Leibler Hamiltonian $\mathcal{H}_L$. In [25,26,12], it was shown how to

deal with the second-order vertex function. Separating small- and large-wave-vector asymptotic behavior, one may show that

$$\Gamma_2(q)\approx\frac{A}{q^2}+Bq^2-\overline{\chi}, \tag{2.6}$$

where

$$A=\frac{3}{2R_G^2f^2(1-f)^2},$$

$$B=\frac{R_G^2}{2f(1-f)}, \tag{2.7}$$

$$\overline{\chi}=2(\chi N-(\chi N)_s)+\left(\frac{3}{f^3(1-f)^3}\right)^{1/2},$$

with $f=N_A/N$ being the volume fraction of the A component. In [12] the third- and fourth-order vertex functions were assumed to be constant. However, as it was noticed in [8,9,27], it is crucial to keep the angle dependence of the fourth-order vertex function in order to discriminate between the parallel and the perpendicular orientations. There, the following approximation was made:

$$\Gamma_3(\mathbf{q}_1,\mathbf{q}_2,\mathbf{q}_3)=\delta(\mathbf{q}_1+\mathbf{q}_2+\mathbf{q}_3)\Gamma_3,$$

$$\Gamma_4(\hat{\mathbf{k}},\hat{\mathbf{q}},-\hat{\mathbf{k}},-\hat{\mathbf{q}})=\lambda(1-\beta(\hat{\mathbf{k}}\cdot\hat{\mathbf{q}})^2),\quad \beta\ll 1, \tag{2.8}$$

where $\hat{\mathbf{k}}=\mathbf{k}/k$. In Eq. (2.8), all the wave vectors are assumed to have the same length $q_0^2=\sqrt{A/B}$, which corresponds to the first unstable mode on the spinodal [2]. The assumption $\beta\ll 1$ was shown to be correct for almost every architecture of AB block-copolymer molecules [27] (for example, for diblocks $\beta\leqslant 0.1$). For an arbitrary star of 4 $\mathbf{q}$'s, one may write to the lowest order in angles [28,29]

$$\begin{aligned}\Gamma_4(\hat{\mathbf{q}}_1,\hat{\mathbf{q}}_2,\hat{\mathbf{q}}_3,\hat{\mathbf{q}}_4)=\delta(\hat{\mathbf{q}}_1+\hat{\mathbf{q}}_2+\hat{\mathbf{q}}_3+\hat{\mathbf{q}}_4)[\lambda_0+\lambda_1((\hat{\mathbf{q}}_1\cdot\hat{\mathbf{q}}_2)\\ \times(\hat{\mathbf{q}}_3\cdot\hat{\mathbf{q}}_4)+(\hat{\mathbf{q}}_1\cdot\hat{\mathbf{q}}_3)(\hat{\mathbf{q}}_2\cdot\hat{\mathbf{q}}_4)+(\hat{\mathbf{q}}_1\cdot\hat{\mathbf{q}}_4)\\ \times(\hat{\mathbf{q}}_2\cdot\hat{\mathbf{q}}_3))+\lambda_2((\hat{\mathbf{q}}_1\cdot\hat{\mathbf{q}}_2)^2+(\hat{\mathbf{q}}_1\cdot\hat{\mathbf{q}}_3)^2\\ +(\hat{\mathbf{q}}_1\cdot\hat{\mathbf{q}}_4)^2+(\hat{\mathbf{q}}_2\cdot\hat{\mathbf{q}}_3)^2+(\hat{\mathbf{q}}_2\cdot\hat{\mathbf{q}}_4)^2\\ +(\hat{\mathbf{q}}_3\cdot\hat{\mathbf{q}}_4)^2)],\\ \frac{\lambda_1}{\lambda_0},\frac{\lambda_2}{\lambda_0}\ll 1.\end{aligned} \tag{2.9}$$

Comparison with Eq. (2.8) gives

$$\lambda=\lambda_0+\lambda_1+2\lambda_2,\quad \beta=-\frac{2\lambda_1+4\lambda_2}{\lambda_0+\lambda_1+2\lambda_2}. \tag{2.10}$$

Thus, the required real-space representation of the Hamiltonian $\mathcal{H}$ may be written as

$$\begin{aligned}N\mathcal{H}[\phi]=\int d\mathbf{r}\Bigg[&\frac{B}{2}(\nabla\phi(\mathbf{r}))^2-\frac{1}{2}\overline{\chi}\phi(\mathbf{r})^2+\frac{A}{2}\int d\mathbf{r}'\mathcal{G}(\mathbf{r}-\mathbf{r}')\\ &\times\phi(\mathbf{r})\phi(\mathbf{r}')+\frac{\Gamma_3}{3!}\phi(\mathbf{r})^3+\frac{\lambda_0}{4!}\phi(\mathbf{r})^4\\ &+\frac{3\lambda_1}{4!}\frac{(\nabla\phi(\mathbf{r})\cdot\nabla\phi(\mathbf{r}))^2}{q_0^4}\\ &+\frac{6\lambda_2}{4!}\phi(\mathbf{r})^2\frac{(\nabla_\alpha\nabla_\beta\phi(\mathbf{r}))^2}{q_0^4}-h(\mathbf{r})\phi(\mathbf{r})\Bigg]+N\mathcal{H}_s,\end{aligned} \tag{2.11}$$

where

$$\mathcal{G}(\mathbf{r}-\mathbf{r}')=\int_q\frac{e^{i\mathbf{q}\cdot(\mathbf{r}-\mathbf{r}')}}{q^2}. \tag{2.12}$$

Here, we have added an auxiliary field h, which will help us to construct a thermodynamical potential governing the dynamics under shear. Afterwards it will be set to zero.

The Fokker-Planck Eq. (2.3) together with Eqs. (2.11,2.7,2.5) form a phenomenological set of equations describing the dynamics of block-copolymer melt under shear flow in the presence of surfaces. We do not solve these equations directly, but following [8] we use the method of Zwanzig [30] to derive a system of coupled equations for the first two cumulants of $P[\phi,t]$

$$c(\mathbf{r})=\langle\phi(\mathbf{r})\rangle,$$

$$S(\mathbf{r}_1,\mathbf{r}_2)=\langle\phi(\mathbf{r}_1)\phi(\mathbf{r}_2)\rangle-\langle\phi(\mathbf{r}_1)\rangle\langle\phi(\mathbf{r}_2)\rangle, \tag{2.13}$$

where c is the average order-parameter profile, and the structure factor S is a measure of the fluctuation strength. We introduce a generating functional

$$G[\xi,t]=\log\int\mathcal{D}\phi\exp\left[\int d\mathbf{r}\,\phi(\mathbf{r})\xi(\mathbf{r})\right]P[\phi,t], \tag{2.14}$$

use Eq. (2.3) to derive an equation of motion for $G[\xi,t]$, and then expand this equation in terms of ξ. The two lowest-order equations read

$$\frac{1}{\mu}\frac{\partial c(\mathbf{r})}{\partial t}=-\frac{D}{\mu}y\frac{\partial c(\mathbf{r})}{\partial x}+B\Delta c(\mathbf{r})+\overline{\chi}c(\mathbf{r})-A\int d\mathbf{r}'\,\mathcal{G}(\mathbf{r}-\mathbf{r}')c(\mathbf{r}')-\frac{\Gamma_3}{2}[c(\mathbf{r})^2+S(\mathbf{0})]-\frac{\lambda_0}{3!}[c(\mathbf{r})^2+3S(\mathbf{0})]c(\mathbf{r})$$
$$+\frac{\lambda_1}{2q_0^4}[\nabla_\alpha(\nabla_\alpha c(\mathbf{r})\{\nabla c(\mathbf{r})\}^2)+\tilde{S}_{\alpha\alpha}\Delta c(\mathbf{r})]-\frac{\lambda_2}{2q_0^4}[c(\mathbf{r})(\nabla_\alpha\nabla_\beta c(\mathbf{r}))^2+c(\mathbf{r})\tilde{S}+\nabla_\alpha\nabla_\beta(c(\mathbf{r})^2\nabla_\alpha$$
$$\times\nabla_\beta c(\mathbf{r}))+S(\mathbf{0})\Delta^2 c(\mathbf{r})]-\frac{2\lambda_1+4\lambda_2}{q_0^4}(\nabla_\alpha\nabla_\beta c(\mathbf{r}))\tilde{S}_{\alpha\beta}+h(\mathbf{r})+(H_1-a_1c(\mathbf{r}))\left[\delta\left(y+\frac{L}{2}\right)+\delta\left(y-\frac{L}{2}\right)\right], \tag{2.15}$$

and

$$\frac{1}{2\mu}\frac{\partial S(\mathbf{r}-\mathbf{r}_1)}{\partial t}=\delta(\mathbf{r}-\mathbf{r}_1)-\frac{D}{\mu}y\frac{S(\mathbf{r}-\mathbf{r}_1)}{\partial x}+B\Delta S(\mathbf{r}-\mathbf{r}_1)+\overline{\chi}S(\mathbf{r}-\mathbf{r}_1)-A\int d\mathbf{r}'\,\mathcal{G}(\mathbf{r}-\mathbf{r}')S(\mathbf{r}'-\mathbf{r}_1)-\frac{\Gamma_3}{2}$$
$$\times[S(\mathbf{0})+2c(\mathbf{r})S(\mathbf{r}-\mathbf{r}_1)]-\frac{\lambda_0}{2}[c(\mathbf{r})^2+S(\mathbf{0})]S(\mathbf{r}-\mathbf{r}_1)-\frac{\lambda_1+2\lambda_2}{q_0^4}\tilde{S}_{\alpha\beta}\nabla_\alpha\nabla_\beta S(\mathbf{r}-\mathbf{r}_1)+\frac{\lambda_1}{2q_0^4}$$
$$\times\nabla_\alpha[2(\nabla_\alpha c(\mathbf{r}))(\nabla c(\mathbf{r})\cdot\nabla S(\mathbf{r}-\mathbf{r}_1))+(\nabla_\alpha S(\mathbf{r}-\mathbf{r}_1))(\nabla c(\mathbf{r}))^2+\tilde{S}_{\beta\beta}\nabla_\alpha S(\mathbf{r}-\mathbf{r}_1)]-\frac{\lambda_2}{2q_0^4}[S(\mathbf{r}-\mathbf{r}_1)$$
$$\times(\nabla_\alpha\nabla_\beta c(\mathbf{r}))^2+S(\mathbf{r}-\mathbf{r}_1)\tilde{S}+2c(\mathbf{r})(\nabla_\alpha\nabla_\beta c(\mathbf{r}))(\nabla_\alpha\nabla_\beta S(\mathbf{r}-\mathbf{r}_1))+S(\mathbf{0})\Delta^2 S(\mathbf{r}-\mathbf{r}_1)+2\nabla_\alpha\nabla_\beta(c(\mathbf{r})S(\mathbf{r}-\mathbf{r}_1)$$
$$\times\nabla_\alpha\nabla_\beta c(\mathbf{r}))+\nabla_\alpha\nabla_\beta(c(\mathbf{r})^2\nabla_\alpha\nabla_\beta S(\mathbf{r}-\mathbf{r}_1))]-a_1S(\mathbf{r}-\mathbf{r}_1)\left[\delta\left(y+\frac{L}{2}\right)+\delta\left(y-\frac{L}{2}\right)\right], \tag{2.16}$$

where

$$\tilde{S}_{\alpha\beta}=\nabla'_\alpha\nabla'_\beta S(\mathbf{r}-\mathbf{r}')|_{\mathbf{r}'=\mathbf{r}},\quad \tilde{S}=\nabla_\alpha\nabla_\beta\nabla'_\alpha\nabla'_\beta S(\mathbf{r}-\mathbf{r}')|_{\mathbf{r}'=\mathbf{r}}. \tag{2.17}$$

Here, we have neglected all higher cumulants and made use of a natural assumption $S(\mathbf{r}_1,\mathbf{r}_2)=S(\mathbf{r}_1-\mathbf{r}_2)$.

Apart from the surface terms, Eqs. (2.15, 2.16) are the real-space analog of the Eqs. (2.25–26) from [8]. Here, the terms proportional to $S(\mathbf{0})$ play the role of the fluctuation integral $\sigma(\hat{\mathbf{k}})$ from [8]:

$$\sigma(\hat{\mathbf{k}})=\frac{\lambda}{2}\int_q S(\mathbf{q})[1-\beta(\hat{\mathbf{k}}\cdot\hat{\mathbf{q}})^2]. \tag{2.18}$$

To keep our model as simple as possible, we leave only the linear term in the surface energy (2.5) and put $a_1=0$. Then we set

$$c(\mathbf{r})=2a\cos(q_0\mathbf{n}\cdot\mathbf{r}+\varphi), \tag{2.19}$$
$$h(\mathbf{r})=2h\cos(q_0\mathbf{n}\cdot\mathbf{r}+\varphi),$$

where a is yet to be determined amplitude, $\mathbf{n}$ is a unit vector perpendicular to the surface of the lamellae, and φ is a phase shift that will be chosen to minimize the surface energy. The auxiliary field h simply follows the behavior of c. Fredrickson has shown [12] that in equilibrium, the presence of the surfaces causes spatial variations of the amplitude a that decay exponentially away from the surface. Since we are only interested in the orientation of the lamellar profile (2.19), we ignore the spacial dependence of a and set it constant. With these simplifications, the equation for the Fourier transform $S(\mathbf{k})$ of $S(\mathbf{r}_1-\mathbf{r}_2)$ from Eq. (2.16) reads

$$\frac{1}{2\mu}\frac{\partial S(\mathbf{k})}{\partial t}=1+\frac{D}{2\mu}k_x\frac{\partial S(\mathbf{k})}{\partial k_y}-S_0^{-1}(\mathbf{k})S(\mathbf{k}), \tag{2.20}$$

where

$$S_0^{-1}(\mathbf{k})=r-\hat{\mathbf{k}}\cdot\vec{\mathbf{e}}\cdot\hat{\mathbf{k}}+Bk^2+\frac{A}{k^2}-\overline{\chi}_s,$$
$$r-\hat{\mathbf{k}}\cdot\vec{\mathbf{e}}\cdot\hat{\mathbf{k}}=2((\chi N)_s-\chi N)+\lambda a^2(1-\beta(\mathbf{n}\cdot\hat{\mathbf{k}})^2)+\sigma(\hat{\mathbf{k}}). \tag{2.21}$$

Here, we have introduced the same notation as in [8,9]. In Eq. (2.21), $S_0(\mathbf{k})$ is the equilibrium structure factor and $r-\hat{\mathbf{k}}\cdot\vec{\mathbf{e}}\cdot\hat{\mathbf{k}}$ denotes the *renormalized* temperature. Within the fluctuation theory, the spinodal temperature determined from the condition

$$r-\hat{\mathbf{k}}\cdot\vec{\mathbf{e}}\cdot\hat{\mathbf{k}}|_{a=0}=0 \tag{2.22}$$

differs from the mean-field value $(\chi N)_s$. In the case $\beta=0$, such a fluctuation correction was discussed in [31]. The presence of shear breaks the rotational symmetry and the spinodal temperature becomes *orientation dependent*. This gives

rise to the $-\hat{\mathbf{k}}\cdot\vec{\mathbf{e}}\cdot\hat{\mathbf{k}}$ term, with $e_{ij}\sim\beta$ [see Eq. (2.8)]. Here, the role of the angle dependency in Γ_4 is especially transparent: if $\beta=0$, we would not be able to discriminate between different orientations.

The method of characteristics [32] gives a formal solution for the Eq. (2.20)

$$S(\mathbf{k},t)=\mu\int_0^t d\tau\exp\left[-\mu\int_0^\tau ds\, S_0^{-1}\left(k_x,k_y+\frac{1}{2}Dsk_x,k_z\right)\right]. \tag{2.23}$$

The steady-state regime is approached as $t\to\infty$. The integration in Eq. (2.23) may be performed in the limiting cases $D\to 0$ and $D\to\infty$ and will be discussed in the next section.

Now we derive an equation for the amplitude a. We substitute the lamellar profile (2.19) into Eq. (2.15) and perform an averaging over the lamellar period

$$\langle\cdots\rangle=\frac{n_x n_y n_z q_0^3}{(2\pi)^3}\int_0^{2\pi/q_0 n_x}dx\int_0^{2\pi/q_0 n_y}dy\int_0^{2\pi/q_0 n_z} \times dz\cos(q_0\mathbf{n}\cdot\mathbf{r}+\varphi)\cdots. \tag{2.24}$$

Discarding the transverse orientations with $n_x\neq 0$ [24,7,8], we obtain

$$\frac{1}{\mu}\frac{\partial a}{\partial t}=h-(r-\mathbf{n}\cdot\vec{\mathbf{e}}\cdot\mathbf{n})a+\frac{1}{2}\lambda(1-\beta)a^3+\eta\cos(\varphi)\,\delta_{n_y^2,1}, \tag{2.25}$$

where $\eta=H_1 q_0/\pi$, and $\delta_{n_y^2,1}$ is the Kronecker delta-symbol that is nonzero only for the parallel ($|n_y|=1$) orientation. Following [8], we notice that Eq. (2.25) has a gradient form (with $h=0$)

$$\frac{1}{\mu}\frac{\partial a}{\partial t}=-\frac{1}{2}\frac{\partial\Phi}{\partial a}. \tag{2.26}$$

Since the potential Φ can only decrease with time

$$\frac{\partial\Phi}{\partial t}=\frac{\partial\Phi}{\partial a}\frac{\partial a}{\partial t}=-\frac{\mu}{2}\left(\frac{\partial\Phi}{\partial a}\right)^2<0, \tag{2.27}$$

the steady-state of the system will be determined by the minimum of Φ. Now we use the auxiliary field h to construct Φ. In steady-state $\partial a/\partial t=0$, and Φ is obtained by integrating

$$h=\frac{1}{2}\frac{\partial\Phi}{\partial a}. \tag{2.28}$$

Using h from Eq. (2.25), we obtain

$$\Phi=\Phi_0-2\eta a\,\delta_{n_y^2,1}, \tag{2.29}$$

where

$$\Phi_0=-\frac{1}{4}\lambda(1-\beta)a^4+2\int_0^a da'(r-\mathbf{n}\cdot\vec{\mathbf{e}}\cdot\mathbf{n})a'. \tag{2.30}$$

In Eq. (2.29), we have already minimized with respect to the phase-shift φ, assuming that $a>0$ (the other terms depend only on even powers of a and are not influenced by this choice).

The nontrivial dependency of $r-\mathbf{n}\cdot\vec{\mathbf{e}}\cdot\mathbf{n}$ on a comes from the term proportional to $\sigma(\hat{\mathbf{k}})$ in Eq. (2.21) and the potential Φ appears to be dependent on the fluctuation integral via Eq. (2.30). Now we are ready to discuss the stable orientations in different regimes.

III. PHASE TRANSITIONS

A. Crossover from small- to high-shear rate behavior

In this section, we analyze the transition from the parallel to perpendicular orientation caused by increase of shear rate (the *A* transition in Fig. 1). We start with noticing that at low shear rates, the parallel orientation is the only stable one. Indeed, as it was shown by Fredrickson [8], Φ_0 is minimal for $n_y^2=1$ in the limit $D\to 0$. The surface term in Eq. (2.29) also favors the parallel orientation. Thus, our theory does not modify Fredrickson's prediction for small shear rates.

At high shear rates $D\to\infty$, the integration in Eq. (2.23) may be performed [24], yielding

$$S_\infty(\mathbf{k})=c_0\left(\frac{\mu q_0^2}{\sqrt{\alpha}D|k_x k_y|}\right)^{2/3}, \tag{3.1}$$

where

$$c_0=\frac{\Gamma\left(\frac{1}{3}\right)}{(9\pi)^{1/3}}\quad\text{and}\quad\alpha=\frac{q_0^2 B}{\pi}. \tag{3.2}$$

For the intermediate shear rates, $S(\mathbf{k})$ may be interpolated between S_0 and S_∞ [7]

$$S(\mathbf{k})=\left[r-\hat{\mathbf{k}}\cdot\vec{\mathbf{e}}\cdot\hat{\mathbf{k}}+Bk^2+\frac{A}{k^2}-\overline{\chi_s}+\frac{1}{c_0}\left(\frac{\sqrt{\alpha}D|k_x k_y|}{\mu q_0^2}\right)^{2/3}\right]^{-1}. \tag{3.3}$$

One should realize that the previous equation is an analytic continuation of the $D\to\infty$ behavior to $D<\infty$ values. As a result, a small-D behavior of Eq. (3.3) does not correspond to the $D\to 0$ behavior of Eq. (2.23). On contrary, it describes the $D\sim O(1)$ region. Since we expect the *A* transition to lay in between the $D\sim O(1)$ and $D\to\infty$ regions, we need to calculate the fluctuation integral $\sigma(\hat{\mathbf{k}})$ in between these regions. This may be done in several steps. First, we use $S(\mathbf{k})$ from Eq. (3.3) to perform the radial part of the integral in Eq. (2.18). This gives

$$\sigma(\hat{\mathbf{k}}) \approx \frac{\lambda q_0^2 \sqrt{c_0}}{16\pi^3}\left(\frac{\mu}{D\sqrt{\alpha}}\right)^{1/3} \int d\Omega \, \frac{1-\beta(\hat{\mathbf{k}}\cdot\hat{\mathbf{q}})^2}{|\hat{q}_x \hat{q}_y|^{1/3}} \times \left[\frac{\pi}{2} + \arctan\left(\frac{q_0\sqrt{c_0}}{|\hat{q}_x\hat{q}_y|^{1/3}}\left(\frac{\mu}{D\sqrt{\alpha}}\right)^{1/3}\right)\right]. \quad (3.4)$$

As a next step, we expand the integrand for $D \ll 1$ and $D \gg 1$ and sum these expressions keeping only the few first terms. Integration over the orientations of the unit vector $\hat{\mathbf{q}}$ ($\int d\Omega \equiv \int_0^\pi d\theta \sin(\theta) \int_0^{2\pi} d\phi$) then gives

$$\sigma(\hat{\mathbf{k}}) = \frac{\lambda}{64\pi^{5/2}}\sqrt{\frac{\alpha}{B^3}}\Bigg\{ -4\pi\left(1-\frac{\beta}{3}\right) + \frac{1}{3Z^3}[I_1 - \beta(I_2(\hat{k}_x^2 + \hat{k}_y^2) + I_3\hat{k}_z^2)] + 4\pi^2 2^{1/3}\sqrt{3}Z\left[1 - \frac{\beta}{7}(2\hat{k}_x^2 + 2\hat{k}_y^2 + 3\hat{k}_z^2)\right] + Z^2[I_4 - \beta(I_5(\hat{k}_x^2+\hat{k}_y^2) + I_6\hat{k}_z^2)]\Bigg\}, \quad (3.5)$$

where

$$Z = \sqrt{4\pi c_0}\left[\frac{\sqrt{\alpha}}{\lambda}\frac{D_*}{D}\right]^{1/3}, \quad D_* = \lambda\mu\sqrt{\alpha},$$

$$I_1 = 2\frac{\sqrt{\pi}\Gamma\left(\frac{5}{6}\right)^2}{\Gamma\left(\frac{13}{6}\right)}, \quad I_2 = 2\frac{\sqrt{\pi}\Gamma\left(\frac{5}{6}\right)\Gamma\left(\frac{11}{6}\right)}{\Gamma\left(\frac{19}{6}\right)},$$

$$I_3 = 2\frac{\Gamma\left(\frac{5}{6}\right)^2\Gamma\left(\frac{3}{2}\right)}{\Gamma\left(\frac{19}{6}\right)},$$

$$I_4 = \frac{\Gamma\left(\frac{1}{6}\right)^3}{\sqrt{\pi}}, \quad I_5 = 2\frac{\sqrt{\pi}\Gamma\left(\frac{1}{6}\right)\Gamma\left(\frac{7}{6}\right)}{\Gamma\left(\frac{11}{6}\right)}, \quad I_6 = 2\frac{\Gamma\left(\frac{3}{2}\right)\Gamma\left(\frac{1}{6}\right)^2}{\Gamma\left(\frac{11}{6}\right)}.$$

This procedure relies on a number of approximations. However, any direct analysis of Eq. (2.23) is impossible and we use Eq. (3.5) for moderate shear rates.

Since Eq. (3.5) does not depend on the renormalized temperature, the integration in Eq. (2.30) is trivial and gives

$$\Phi = [\tau + \sigma(\mathbf{n})]a^2 + \frac{1}{4}\lambda a^4(1-\beta) - 2\eta a\,\delta_{n_y^2,1}, \quad (3.6)$$

where

$$\tau = 2((\chi N)_s - \chi N).$$

Minimization with respect to a gives to the first order in η

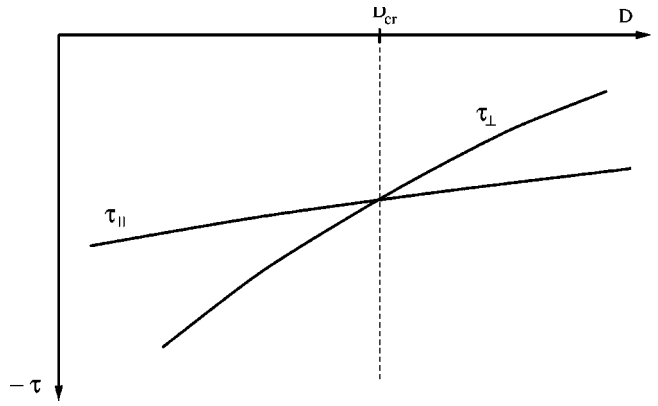

FIG. 3. Schematic behavior of the spinodal temperatures for the parallel and perpendicular orientations in the vicinity of the crossover point.

$$\Phi = -\frac{[\tau+\sigma(\mathbf{n})]^2}{\lambda(1-\beta)} - 2\eta\sqrt{-2\frac{\tau+\sigma(\mathbf{n})}{\lambda(1-\beta)}}\delta_{n_y^2,1}. \quad (3.7)$$

The order-disorder transition (ODT) occurs when Φ becomes negative. The corresponding transition temperature is

$$\tau_s(\mathbf{n}) = -\sigma(\mathbf{n}), \quad (3.8)$$

which coincides with Eq. (2.22). The orientation with the lowest σ will appear immediately below the ODT temperature. The crossover (the A transition) is then located at such a value of D that $\sigma_\parallel - \sigma_\perp$ changes its sign. From Eq. (3.5), this point is given by

$$\sigma_\parallel - \sigma_\perp \sim \frac{1}{3Z^2}(I_3 - I_2) + \frac{4\pi^2}{7}2^{1/3}\sqrt{3}Z + Z^2(I_6 - I_5) = 0, \quad (3.9)$$

and is found to be

$$D_{cr} \approx 4\times 10^3 \mu\alpha. \quad (3.10)$$

From Eq. (3.9) it also follows that $\tau_s^\parallel > \tau_s^\perp$ for $D < D_{cr}$, which fits the weak-shear behavior discussed in the beginning of this section. When $D > D_{cr}$, the perpendicular orientation first appear below the spinodal. This crossover is depicted in Fig. 3.

As it was noticed before [7,8], the mean-field behavior is restored in the limit $D \to \infty$. On the other hand, the small-D region is dominated by fluctuations. Thus, D_{cr} may be interpreted as a position of a crossover from the fluctuation to mean-field behavior. The scaling properties of D_{cr} follow from Eq. (3.10) and are determined by the Onsager coefficient μ. Using the results of [33–36]($\mu \equiv q_0^2\lambda(q_0)/N$ with λ from [34,35]) we obtain

$$D_{cr} \sim N^{-3}, \quad (3.11)$$

which shows that the fluctuation region disappears in the limit $N \to \infty$. In equilibrium, the same conclusion was drawn in [2,31].

Finally, we emphasize that the results of this section are independent of the surface interaction. The same results may be obtained within the Fredrickson theory [8] ($\eta=0$).

B. B and C transitions

In the previous section, we have discussed the order-disorder transitions. Now we consider lower temperatures and look for transitions between different orientations in the strong-shear limit. The corresponding free energies are given by Eq. (3.7)

$$\Phi_{\parallel}=-\frac{(\tau+\sigma_{\parallel})^2}{\lambda(1-\beta)}-2\eta\sqrt{-2\frac{\tau+\sigma_{\parallel}}{\lambda(1-\beta)}}, \qquad (3.12)$$

$$\Phi_{\perp}=-\frac{(\tau+\sigma_{\perp})^2}{\lambda(1-\beta)},$$

where $\sigma(\mathbf{n})$ is given by its high-shear limit of Eq. (3.5)

$$\sigma(\mathbf{n})=\frac{(\alpha\lambda)^{2/3}}{B^{3/2}}\left(\frac{D_*}{D}\right)^{1/3}\frac{2^{1/3}\sqrt{3}}{8}\sqrt{c_0}\left[1-\frac{\beta}{7}(2n_y^2+3n_z^2)\right]. \qquad (3.13)$$

To the leading order in D_*/D, the transition from the perpendicular to parallel orientation occurs at temperatures that are the roots of the equation $\Phi_{\parallel}=\Phi_{\perp}$

$$\tau_1=-\sigma_{\parallel}-\frac{(\sigma_{\parallel}-\sigma_{\perp})^4}{8\eta^2\lambda(1-\beta)},$$

$$\tau_2=-\frac{2\eta^2\lambda(1-\beta)}{(\sigma_{\parallel}-\sigma_{\perp})^2}, \quad \text{if} \quad \eta^2\lambda(1-\beta)>(\sigma_{\parallel}-\sigma_{\perp})^3, \qquad (3.14)$$

where

$$\sigma_{\parallel}-\sigma_{\perp}=\beta\frac{2^{1/3}\sqrt{3c_0}}{56}\frac{(\alpha\lambda)^{2/3}}{B^{3/2}}\left(\frac{D_*}{D}\right)^{1/3}. \qquad (3.15)$$

There, τ_1 corresponds to the $\perp\rightarrow\parallel$ transition, while τ_2 to the reverse one. Now we summarize our results in a phase diagram.

IV. DISCUSSION OF THE PHASE DIAGRAM AND CONCLUSION

In this paper, we incorporated some real-system properties into the previously developed theory of the orientational phase transitions under shear flow [7–9]. In particular, we considered the influence of the shear-cell boundaries in the gradient direction on the orientation of the lamellar phase. In equilibrium, the lamellae are known to orient parallel with respect to the boundaries [12,13]. Under shear, the tendency to orient parallel to the surfaces competes with the orientation favored by the flow that appears as a result of the coupling between the flow velocity field and the order-parameter fluctuations [7,8]. The interplay between these two factors produces the nontrivial phase diagram shown in Fig. 4.

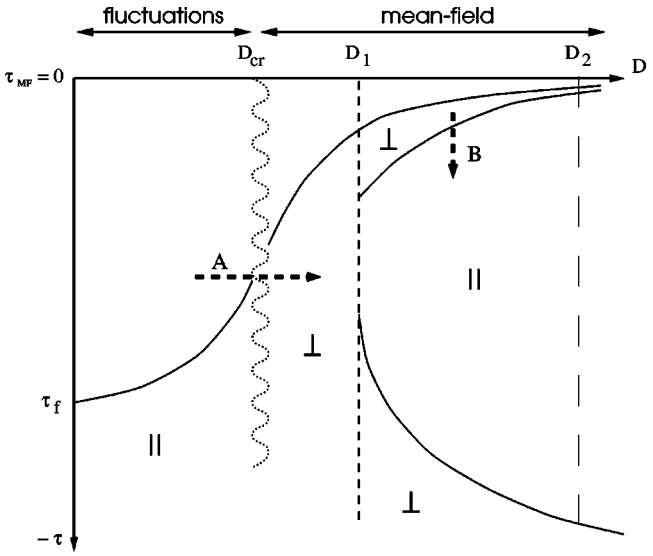

FIG. 4. Phase diagram for the lamellar phase under steady simple shear flow as predicted in this work.

At low shear rates, the parallel orientation is preferred by both the shear and surface terms in Eq. (2.29). Therefore, it is the only stable orientation in that part of the phase diagram. When shear rate reaches the value D_{cr} given by Eq. (3.10), the perpendicular orientation becomes stable immediately below the ODT temperature. We associate this change in orientation with the crossover from the fluctuation-dominated behavior to the mean-field one. Indeed, at very small shear rates, the equilibrium fluctuation spectrum is only slightly modified by the flow, while at high shear rates, the flow strongly suppresses fluctuations and restores the mean-field behavior. Therefore, there is a crossover point and the corresponding change of orientation.

At high shear rates and away from the spinodal, the surface influence starts to play an important role. In the narrow region between D_{cr} and D_1, estimated from the condition in Eq. (3.14)

$$D_1=2\frac{(3c_0)^{3/2}}{56^3}\frac{\beta}{1-\beta}D_*\frac{\lambda\alpha^2}{\eta^2B^{9/2}},$$

the influence of shear is still very strong and is capable of stabilizing the perpendicular orientation at all temperatures. The size of this region is very small due to the scaling $D_1\sim N^{-13/2}$. When $D>D_1$, there appears a region where the parallel orientation is stable. It takes over the perpendicular one at $\tau=\tau_1$ and looses its stability again at $\tau=\tau_2$ given by Eq. (3.14). This region grows as the shear rate increases, and in the limit $D=\infty$, the parallel orientation occupies the whole range of temperatures $(0,-\infty)$. This coincides with the predictions of the equilibrium mean-field theory [12,13]. We therefore argue that there is no sharp C transition as shown in Fig. 1. Since the region between the spinodal and the parallel phase shrinks with an increase of the shear rate, there will always be some value D_2 such that for $D>D_2$ the size of this region will be smaller than the resolution of the experi-

mental device. This value D_2 may be misinterpreted as a position of an additional transition.

An important feature of our theory is that it is able to reproduce the *B* transition without additional assumptions. In the previous theory [8], Fredrickson had to take into account the difference in viscosities of the pure components in order to reproduce the *B* transition. Namely, he put $\eta[\phi]=\eta_0+\eta_1\phi$, which may be considered as a Taylor expansion of the viscosity $\eta[\phi]$. As a result, in strong-shear limit, the size of the stability region for the perpendicular phase is of order of $(\eta_0/\eta_1)^2$ and grows as $D\to\infty$. While depicting the main physics, this approach has internal problems since the derivative η_1 is not a well-defined object and therefore, the whole theory depends on a phenomenological parameter that is difficult to estimate. Moreover, Fredrickson's theory does not predict the C transition. Our theory is free from these problems. It, however, predicts the $\|\to\perp$ transition at very low temperatures in strong-shear limit, which was not observed. There could be several explanations of this prediction. First, this transition occurs at very low temperatures (τ_2) where the weak-segregation theory does not work. Second, this transition might be an artifact of the $O(\eta)$ expansion. Finally, this transition may be removed if we use Fredrickson's argument about the viscosity dependence on the order parameter. It stabilizes the parallel orientation at low temperatures.

It is possible that the absolute value of the surface interaction is small. However, since it acts as a *symmetry-breaking* factor, its influence is very important [14,15]. This statement may be checked experimentally. We have shown that the positions of the transition lines in the strong-shear limit are dependent on the strength of the surface-copolymer interaction $\eta\sim(\chi N)_{cop\text{-}surf}$. Therefore, the phase diagram of a particular copolymer system depends on the material of the shear-cell walls. A systematic study of this dependency will provide arguments for or against our theory.

In this paper, we have considered the influence of the walls in the gradient direction. We also want to comment on the role of the boundaries in the other shear directions (flow and vorticity). Formally, these walls will also induce alignment parallel to themselves. However, the flow profile near those walls is no longer a simple triangular one and we expect this disordered flow to destroy their orientational tendency. Moreover, the distance between those surfaces is normally much larger than between the walls in the gradient direction and their influence is thus weaker. Therefore, we neglected them in our work.

Finally, we want to discuss, briefly, possible modifications and extensions of the developed theory. A very interesting problem is to calculate the alterations of the density profile in a confined system under shear. This may be achieved by restoring the position dependency in the amplitude *a* and deriving the corresponding amplitude equation from Eq. (2.15). In the absence of shear, this problem was solved in [12]. Another possibility is to use our formalism for other external fields rather than interactions with surfaces. A good example is an electric field that is coupled to the square of the order parameter [37,38]. With some modifications Eqs. (2.15, 2.16) may be a starting point for the corresponding theory. The importance of such a theory for a system in electric field and simultaneously under shear was outlined in [38].

ACKNOWLEDGMENT

The authors want to express their gratitude to Evgeny Polushkin for helpful discussions of the experimental details.

APPENDIX: INFLUENCE OF THERMAL FLUCTUATIONS

Here, we want to emphasize the role of fluctuations in our theory. We are going to show that if the Fokker-Planck Eq. (2.3) is replaced by a deterministic one, the theory will not be able to discriminate between different orientations. What follows should not be considered as a proof but, more likely, as an illustration that has general features.

Let us consider a Langevin equation equivalent to the Fokker-Planck Eq. (2.3). If we now remove the noise term, it reads

$$\frac{\partial\phi}{\partial t}+\mathbf{v}\cdot\boldsymbol{\nabla}\phi=\tilde{\mu}\boldsymbol{\nabla}^2\frac{\delta\mathcal{H}_L}{\delta\phi}, \tag{A1}$$

where an Onsager mobility $\tilde{\mu}$ differs from μ in Eq. (2.3) and $\mathcal{H}_L$ is the Leibler Hamiltonian [Eq. (2.11)] without $\mathcal{H}_s$ and $h=0$. A similar equation was considered in [39]. There the authors used a Hamiltonian with $\lambda_1=\lambda_2=0$ and showed that in steady state, the theory predicts both orientations to be equally stable at all shear rates. This is not surprising since their theory does not contain fluctuations and the angular dependence of the fourth-order vertex function Γ_4—the two ingredients that were argued to be crucial in explaining the reorientation phenomena [8,9,27].

In order to separate these two effects, we keep the angular dependence in Γ_4 (λ_1, $\lambda_2\neq 0$), but use the deterministic Eq. (A1). We follow the approach of [39] and derive an amplitude equation from Eq. (A1) assuming a single plane-wave density profile. The solution of this equation is

$$A(t)=\left[\frac{P(t)}{A(0)^2}+3P(t)\int_0^t d\tau\, f(\tau)P^{-1}(\tau)\right]^{-1/2}, \tag{A2}$$

and

$$f(t)=1+4Q^4\left(\frac{\lambda_1+2\lambda_2}{\lambda_0}\right),\quad P(t)=\exp\left[-2\int_0^t d\tau\,\sigma(\tau)\right],$$

$$\sigma(t)=(1+\epsilon)Q^2-Q^4-\frac{1}{4},\quad Q^2=q_x^2+(q_y-Dtq_x)^2+q_z^2,$$

where A is the amplitude, $\epsilon=(\overline{\chi}-\overline{\chi_s})/\overline{\chi_s}$, and the amplitude and the units of length and time are scaled with $\sqrt{\overline{\chi_s}/\lambda_0}$, $\sqrt{B/\overline{\chi_s}}$, and $B/(\tilde{\mu}\overline{\chi_s}^2)$, respectively. We see that the equation becomes symmetric with respect to the interchange $q_y\leftrightarrow q_z$.

Thus, even in the presence of the angular dependence in Γ_4, it is impossible to distinguish between the parallel and perpendicular orientations starting from Eq. (A1).

We believe that a theory without fluctuations of the order parameter is not capable of describing the reorientational transitions. There are phenomena where fluctuations only modify a deterministic behavior [40–42]. However, the orientational behavior under shear flow does not belong to this class of phenomena. It can only occur in the presence of thermal fluctuations.

[1] I. Hamley, *The Physics of Block Copolymers* (Oxford University Press, Oxford, New York, 1998).
[2] L. Leibler, Macromolecules **13**, 1602 (1980).
[3] K.A. Koppi *et al.*, J. Phys. II **2**, 1941 (1992).
[4] K.A. Koppi, M. Tirrell, and F.S. Bates, Phys. Rev. Lett. **70**, 1449 (1993).
[5] T. Tepe *et al.*, Macromolecules **28**, 3008 (1995).
[6] G. Schmidt, W. Richtering, P. Lindner, and P. Alexandridis, Macromolecules **31**, 2293 (1998).
[7] M.E. Cates and S.T. Milner, Phys. Rev. Lett. **62**, 1856 (1989).
[8] G.H. Fredrickson, J. Rheol. **38**, 1045 (1994).
[9] A.N. Morozov, A.V. Zvelindovsky, and J.G.E.M. Fraaije, Phys. Rev. E **61**, 4125 (2000).
[10] Y. Zhang, U. Wiesner, and H.W. Spiess, Macromolecules **28**, 778 (1995).
[11] S.S. Patel, R.G. Larson, K.I. Winey, and H. Watanabe, Macromolecules **28**, 4313 (1995).
[12] G.H. Fredrickson, Macromolecules **20**, 2535 (1987).
[13] K. Binder, Adv. Polym. Sci. **138**, 1 (1998).
[14] N.P. Balsara *et al.*, Macromolecules **27**, 2566 (1994).
[15] J.H. Laurer, B.S. Pinheiro, D.L. Polis, and K.I. Winey, Macromolecules **32**, 4999 (1999).
[16] H. Tang and K.F. Freed, J. Chem. Phys. **97**, 4496 (1992).
[17] M. Kikuchi and K. Binder, J. Chem. Phys. **101**, 3367 (1994).
[18] G. Brown and A. Chakrabarti, J. Chem. Phys. **101**, 3310 (1994).
[19] G. Brown and A. Chakrabarti, J. Chem. Phys. **102**, 1440 (1994).
[20] K. Binder, H.L. Frisch, and S. Stepanow, J. Phys. II **7**, 1353 (1997).
[21] M.W. Matsen, J. Chem. Phys. **106**, 7781 (1997).
[22] H.P. Huinink, J.C.M. Brokken-Zijp, M.A. van Dijk, and G.J.A. Sevink, J. Chem. Phys. **112**, 2452 (2000).
[23] G.J.A. Sevink *et al.*, J. Chem. Phys. **110**, 2250 (1999).
[24] A. Onuki and K. Kawasaki, Ann. Phys. (Leipzig) **121**, 456 (1979).
[25] T. Ohta and K. Kawasaki, Macromolecules **19**, 2621 (1986).
[26] M.O. de la Cruz and I.C. Sanchez, Macromolecules **19**, 2501 (1986).
[27] A. Morozov and J. Fraaije, Macromolecules **34**, 6134 (2001).
[28] S.A. Brazovskii, I.E. Dzyaloshinskii, and A.R. Muratov, Zh. Éksp. Teor. Fiz. **68**, 175 (1975) [Sov. Phys. JETP **66**, 625 (1987)].
[29] E.I. Kats, V.V. Lebedev, and A.R. Muratov, Phys. Rep. **228**, 1 (1993).
[30] R. Zwanzig, in *Lecture Notes in Physics, Vol. 132: Systems Far from Equilibrium*, edited by L. Garrido (Springer, New York, 1980), pp. 198–225.
[31] G.H. Fredrickson and E. Helfand, J. Chem. Phys. **87**, 697 (1987).
[32] N. G. van Kampen, *Stochastic Processes in Physics and Chemistry* (North-Holland, Amsterdam, 1981).
[33] K. Kawasaki and K. Sekimoto, Macromolecules **22**, 3063 (1989).
[34] K. Binder, J. Chem. Phys. **79**, 6387 (1983).
[35] G.H. Fredrickson, J. Chem. Phys. **85**, 5306 (1986).
[36] C.-Y. Huang and M. Muthukumar, J. Chem. Phys. **107**, 5561 (1997).
[37] K. Amundson, E. Helfand, X. Quan, and S.D. Smith, Macromolecules **26**, 2698 (1993).
[38] A. Onuki and J. Fukuda, Macromolecules **28**, 8788 (1995).
[39] F. Drolet, P. Chen, and J. Viñals, Macromolecules **32**, 8603 (1999).
[40] I.W. Hamley, Macromol. Theory Simul. **9**, 363 (2000).
[41] S.R. Ren and I.W. Hamley, Macromolecules **34**, 116 (2001).
[42] B.A.C. van Vlimmeren *et al.*, Macromolecules **32**, 646 (1999).